ABC2: Journal of Architecture, Building, Construction, and Cities

Research Article

Urban Heat Island Vulnerability Assessment Using Remote Sensing and Land Surface Temperature Analysis: Evidence from Southern Mehrabad, Tehran

Fateme Gholami[1*], Azadeh Lak[2], Jian Zhong[1]

[1] University of Greenwich, London, United Kingdom.
[2] Shahid Beheshti University, Tehran, Iran.

DOI: https://doi.org/10.66408/abc2.2026.83

* Correspondence: F.gholami@greenwich.ac.uk

Abstract

Urban Heat Islands (UHIs) pose escalating threats to public health, energy systems, and quality of life in rapidly urbanizing cities of the Global South. This paper presents a remote sensing-based thermal diagnostic of Southern Mehrabad—a socioeconomically vulnerable neighborhood in southwestern Tehran located adjacent to Mehrabad Airport, one of the city's most significant heat sources. Using ten-year Landsat 8/9 satellite imagery, Land Surface Temperature (LST) and Normalized Difference Vegetation Index (NDVI) data were extracted and spatially analyzed across the neighborhood. Findings reveal persistent high-temperature clusters in commercial and industrial zones, and a strong inverse correlation between vegetation cover and surface temperature (R^2=0.63). The study demonstrates how satellite-derived thermal mapping, validated through field surveys, can systematically identify UHI hotspots in under-resourced urban neighborhoods. Results provide a data-driven baseline for evidence-based climate-responsive urban planning in comparable Global South contexts.

Received: 27/05/2026
Revised: 02/06/2026
Accepted: 25/06/2026
Published: 15/07/2026

Volume: 2026
Issue: 04
Pages: 61-73

Keywords: Urban Heat Island; Remote Sensing; Land surface temperature; NDVI; Tehran; Landsat

Highlights

- A strong inverse relationship between NDVI and LST confirms vegetation's cooling effect (R^2 = 0.63).
- Thermal hotspots are concentrated in commercial, industrial, and low-vegetation areas of the neighbourhood.

1 Introduction

The 21st century is facing the critical challenge of climate change—a phenomenon that poses serious threats to the global environment and human activities (IPCC, 2023). Climate change is a global phenomenon that involves all regions of the world and has tangible effects on natural and human systems, from water resources to ecosystems, food production, coastlines, industries, human settlements, and public health (IPCC, 2022). Ultimately, these consequences result in profound social, economic, and environmental impacts (UN, 2021).

Among these impacts, global warming stands out as one of the primary contributors to increased urban vulnerability, especially under conditions of rapid urban growth and rising urban populations (Jones et al., 1986). According to NASA's analysis, 2024 was the warmest year on record (NASA, 2025). The average land and ocean surface temperature in that year was about 1.28 °C above the 20th-century baseline (1951–1980), which is approximately 1.47 °C higher than the pre-industrial average (1850–1900) (NASA, 2025). According to the WMO report, 2024 was also confirmed as the warmest year since the beginning of 175 years of recorded observations (WMO, 2025).

A clear and measurable indicator of climate change in cities is the Urban Heat Island (UHI) effect (EPA, 2025a; NLC, 2023)—a condition where urban areas exhibit significantly higher temperatures than their surrounding rural counterparts (Oke, 1982). UHIs are generally classified into two main categories (Kong et al., 2021; Oke et al., 2017): surface UHIs and atmospheric UHIs. The surface UHI refers to temperature differences that occur at or below the ground and includes the subsurface UHI (UHIsub) and the surface UHI (UHIsurf), which are strongly influenced by land cover, material properties, and solar radiation absorption. In contrast, atmospheric UHIs are concerned with the warming of the air above the city and are typically divided into the canopy-layer UHI (UHIUCL), which extends from the ground to the mean building height, and the boundary-layer UHI (UHIUBL), which reaches above the urban canopy into the lower atmosphere. In this study, we specifically investigate surface UHI, focusing on the temperature variations at and near the ground surface.

The UHI effect poses serious threats to urban sustainability, public health, and urban liveability, especially during periods of extreme heat (EPA, 2023). This phenomenon is particularly severe in developing countries, where rapid and unplanned urbanization occurs in the absence of advanced technologies or adequate crisis-management infrastructure. In such conditions, climate change not only threatens the environment but also deepens existing social inequalities and reduces residents' quality of life (Smith et al., 2014).

UHIs significantly affect urban life by impacting public health, energy systems, climate, and the economy (Gartland, 2012). Exposure to extreme heat has risen globally, with 125 million more people affected by heat waves between 2000 and 2016 (WHO, n.d.), and heat stress is projected to cause the loss of 80 million full-time jobs by 2030, particularly in low-income regions such as South Asia and West Africa (ILO, 2019; Kjellström et al., 2016; Zhang et al., 2011). Heat-related mortality is expected to increase substantially, with 92,070 additional deaths by 2030 and 255,486 by 2050 if no adaptation measures are implemented (Stone Jr et al., 2021; WHO, 2014).

Tehran, the capital of Iran, as a sprawling megacity, is a prominent example of these challenges. Rapid urban expansion, high population density, and specific climatic conditions such as air pollution and atmospheric stagnation (due to low wind speeds) have made Tehran increasingly vulnerable to the negative effects of urban heat islands (Sodoudi et al., 2014). Among Tehran's neighbourhoods, some areas face greater vulnerability. Southern Mehrabad—located near Mehrabad Airport and known as one of the prominent heat islands in southwestern Tehran—has long struggled with socio-economic deprivation and now faces additional strain due to intensified thermal stress. This study examines how remote sensing technologies can systematically identify UHI patterns in such vulnerable neighbourhoods and provide actionable insights for climate adaptation.

2 Literature Review: Remote Sensing Methods for UHI Assessment

2.1 Land Surface Temperature (LST) Extraction from Satellite Imagery

Remote sensing provides a cost-effective and comprehensive approach to monitoring urban thermal environments, particularly in data-poor contexts where ground-based weather stations are sparse or unavailable. Satellite-derived Land Surface Temperature (LST) has become the primary indicator for assessing surface UHI intensity (Stewart & Oke, 2012). Landsat 8 and 9, equipped with thermal infrared sensors (TIRS), offer spatially continuous temperature data at 100-meter resolution, making them suitable for neighbourhood-scale analysis (Rizwan et al., 2008).

LST extraction involves converting thermal band digital numbers to at-satellite brightness temperature, followed by emissivity correction to account for surface material properties. Studies in cities such as Patna, India (Yadav et al., 2023) and Khanaqin, Iraq (Nasraldin et al., 2024) have demonstrated the reliability of Landsat-derived LST for identifying thermal hotspots and establishing correlations with land cover characteristics.

2.2 Normalized Difference Vegetation Index (NDVI) and Its Relationship with LST

The Normalized Difference Vegetation Index (NDVI), derived from red and near-infrared spectral bands, serves as a proxy for vegetation density and health. Numerous studies have documented a strong inverse relationship between NDVI and LST, attributing this cooling effect to evapotranspiration and shading provided by vegetation (Bowler et al., 2010; Yu et al., 2018). In arid and semi-arid climates, where vegetation is limited, even small increases in green cover can produce measurable temperature reductions (Weng, 2003).

Research in cities like Patna showed R^2 values exceeding 0.90 for the NDVI-LST relationship (Yadav et al., 2023), while studies in Khanaqin reported moderate correlations ($r = -0.53$, $R^2 = 0.28$) during peak summer months (Nasraldin et al., 2024). These variations underscore the importance of local climate, land use, and vegetation characteristics in moderating surface temperatures.

2.3 Integrating Remote Sensing with Spatial Analysis for UHI Vulnerability Mapping

GIS-based spatial analysis enables researchers to overlay LST and NDVI data with land use, building footprints, and demographic information to identify vulnerable populations and priority intervention zones. Studies combining remote sensing with field validation have shown that satellite-derived thermal maps can accurately reflect ground conditions when calibrated with in situ measurements (Amirtham & Devadas, 2007). This integration is particularly valuable in Global South contexts, where resource constraints limit the availability of extensive ground-based monitoring networks.

3 Study Area and Data

3.1 Southern Mehrabad Neighbourhood Context

Southern Mehrabad is located in southwestern Tehran, District 9, immediately adjacent to Mehrabad International Airport—a major anthropogenic heat source (Figure 1). The neighbourhood covers approximately 2.5 square kilometres and is characterized by informal development patterns, mixed land uses, and significant socioeconomic vulnerability (Azizdoost et al., 2019). The area's proximity to the airport exposes it to aircraft-generated heat, exhaust emissions, and limited vegetation cover due to aviation safety restrictions.

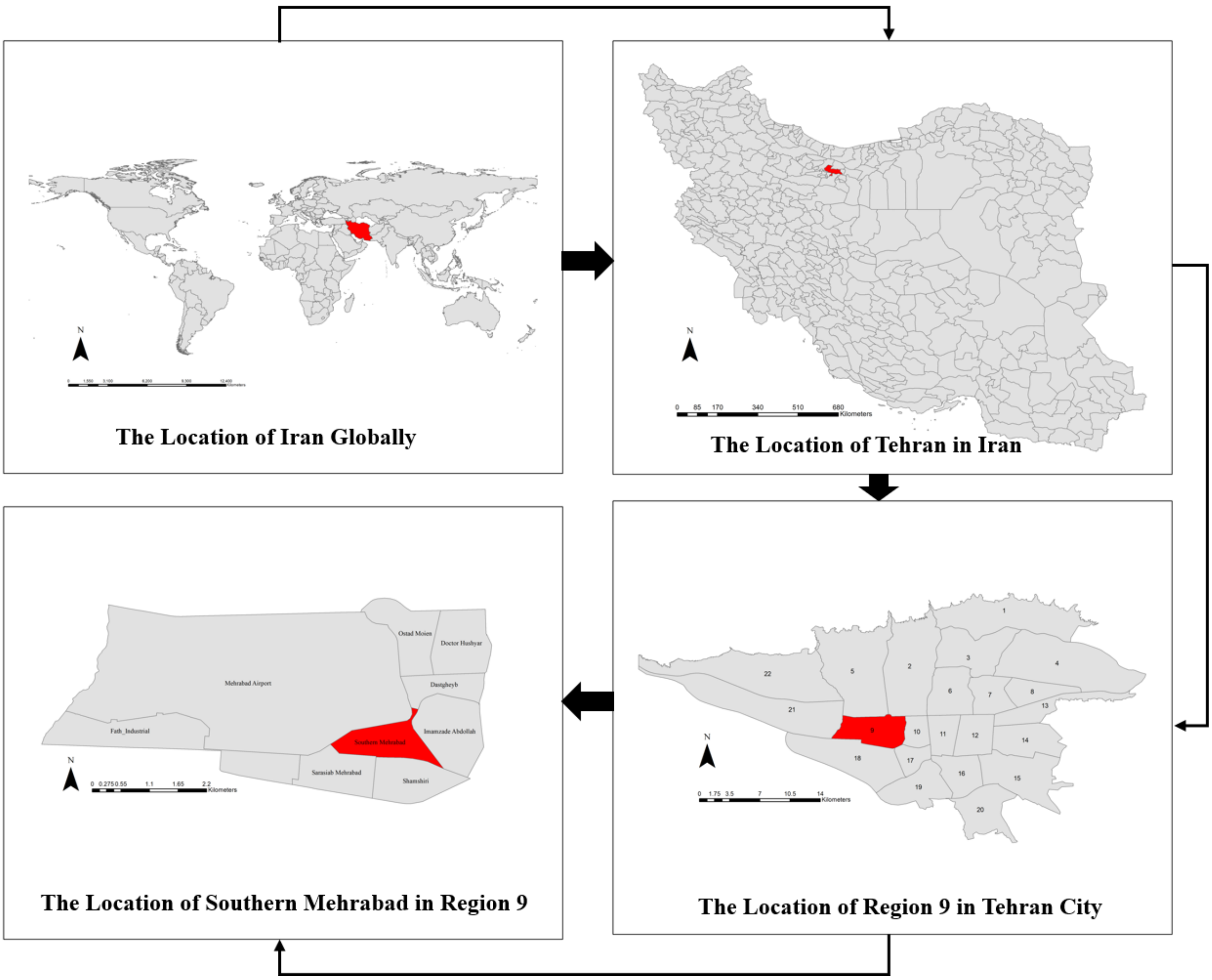

Figure 1. Location of the case study (Southern Mehrabad Neighbourhood) (Source: authors).

The neighbourhood exhibits diverse land uses including residential areas in the core, commercial strips along main roads, scattered industrial facilities, and vacant lots primarily in northern and eastern sections. Building typologies range from low-rise traditional structures to informal settlements, with minimal green space and predominantly impervious surfaces. This morphological complexity, combined with socioeconomic constraints, makes Southern Mehrabad an ideal case study for examining UHI vulnerability in under-resourced urban contexts.

3.2 Satellite Data and Temporal Coverage

This study utilized Landsat 8 and Landsat 9 imagery spanning a ten-year period to capture long-term thermal patterns and seasonal variations. Cloud-free images were selected from summer months (June-August) when UHI effects are most pronounced. Landsat's 16-day revisit cycle and 100-meter thermal resolution (resampled to 30 meters for visualization) provide sufficient spatial and temporal coverage for neighbourhood-scale analysis.

LST data were extracted from thermal infrared bands (Band 10 for Landsat 8/9) using radiometric calibration and emissivity correction algorithms. NDVI was calculated from visible red (Band 4) and near-infrared (Band 5) reflectance values. All processing was conducted using Python programming language on the Google Earth Engine (GEE) platform, which enables efficient cloud computing and temporal aggregation of satellite imagery.

3.3 Ancillary Data and Field Validation

Complementary spatial data were collected from Tehran Municipality GIS repositories, including land use classifications, building footprints, and parcel boundaries. Environmental variables such as humidity, wind speed, and topography were obtained from the Iran Meteorological Organization and Global Wind Atlas to contextualize thermal patterns.

Field surveys were conducted during summer 2023 to validate satellite-derived LST values and document surface material conditions. Portable thermal sensors were used to measure ground temperatures at 50 sampling points distributed across different land use types. The correlation between satellite LST and field measurements yielded an R^2 value of 0.78, confirming the reliability of remote sensing outputs for this study area.

4 Methodology

4.1 LST Extraction and Preprocessing

Land Surface Temperature extraction followed standard radiometric calibration procedures. Digital numbers from Landsat thermal bands were first converted to top-of-atmosphere (TOA) radiance using sensor-specific calibration coefficients. Brightness temperature was then calculated using Planck's law. Finally, emissivity correction was applied using land cover-specific emissivity values derived from NDVI thresholds:

- Water bodies: ε = 0.991
- Vegetation (NDVI > 0.5): ε = 0.973
- Built-up areas (NDVI < 0.2): ε = 0.950
- Mixed surfaces (0.2 ≤ NDVI ≤ 0.5): interpolated values

Cloud masking was performed using Landsat quality assessment bands to exclude contaminated pixels. Temporal compositing techniques were employed to generate seasonal averages and identify persistent thermal hotspots across multiple years.

4.2 NDVI Calculation and Classification

NDVI was calculated using the standard formula:

$$NDVI = \frac{NIR - Red}{NIR + Red} \quad (1)$$

where NIR represents near-infrared reflectance (Band 5) and Red represents red band reflectance (Band 4). NDVI values range from -1 to +1, with higher values indicating denser, healthier vegetation. For this study, NDVI was classified into five categories:

- No vegetation: NDVI < 0.1
- Sparse vegetation: 0.1 ≤ NDVI < 0.3
- Moderate vegetation: 0.3 ≤ NDVI < 0.5
- Dense vegetation: 0.5 ≤ NDVI < 0.7
- Very dense vegetation: NDVI ≥ 0.7

4.3 Spatial Normalization and Analysis in ArcGIS

Spatial analysis was conducted in ArcGIS Pro to integrate LST and NDVI layers with land use and building data. All datasets were reprojected to a common coordinate system (WGS 1984 UTM Zone 39N) and resampled to 30-meter resolution for consistency. Zonal statistics were calculated to determine average LST values for each land use type, building block, and vegetation density class.

Thermal hotspot areas were identified through spatial analysis and visual interpretation of LST distributions derived from satellite imagery. Zones consistently exhibiting the highest temperature values across the study period were classified as hotspots, representing areas where heat is spatially concentrated. These patterns indicate persistent UHI hotspots that require priority intervention.

4.4 Statistical Correlation Analysis

Pearson correlation coefficients were calculated to quantify the relationship between NDVI and LST. Scatter plots with linear regression trend lines were generated using Python's Matplotlib library to visualize the strength and direction of correlations. R^2 values were computed to assess the explanatory power of NDVI in predicting LST variation across the study area.

5 Results

5.1 Ten-Year LST Patterns and Temporal Trends

Analysis of summer LST data from 2014 to 2024 reveals persistent thermal patterns in Southern Mehrabad. As shown in Figure 2, mean neighbourhood LST ranged from 32°C to 38°C during peak summer months, with maximum values exceeding 42°C in specific hotspots. Temporal trends show a gradual increase in average LST of approximately 0.3°C per year, consistent with broader urban warming patterns documented across Tehran (Roshan et al., 2021).

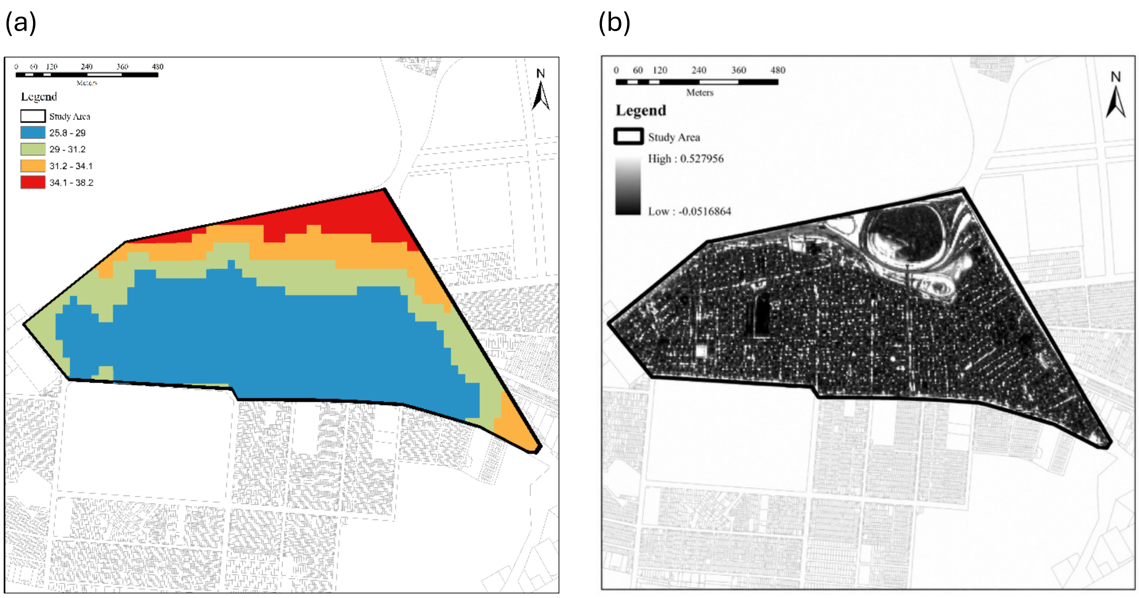

Figure 2. a) Ten-year mean LST of the Southern Mehrabad neighbourhood, highlighting spatial patterns of surface heat intensity; (b) NDVI map of the study area showing the distribution and variability of vegetation cover (Source: authors).

The spatial distribution of LST exhibits clear patterns: the highest temperatures (37–42°C) are concentrated in three zones: (1) commercial areas along the southern edge adjacent to Shahid Eghbali Street, (2) industrial facilities in the eastern fringe near the airport boundary, and (3) vacant lots in the northern and southeastern sections lacking vegetation cover. These hotspots remained stable across the ten-year observation period, indicating structural rather than transient thermal vulnerability.

5.2 NDVI Distribution and Vegetation Cover Patterns

NDVI analysis reveals severe vegetation deficiency across most of Southern Mehrabad. As illustrated in Figure 2, approximately 65% of the neighbourhood exhibits NDVI values below 0.2, classified as having no or minimal vegetation. Only 12% of the area shows moderate to dense vegetation (NDVI > 0.3), concentrated primarily in small parks, residential courtyards, and street tree alignments in the central residential zone.

The spatial distribution of vegetation is highly fragmented. Northern vacant lots and eastern industrial areas register NDVI values near zero, while pockets of moderate vegetation (NDVI 0.3–0.5) exist in older residential blocks where traditional courtyard houses retain small gardens. No areas achieve NDVI values above 0.7, reflecting the overall scarcity of substantial green infrastructure.

5.3 NDVI-LST Correlation: Quantifying the Cooling Effect of Vegetation

Statistical analysis in Figure 3 demonstrates a strong inverse relationship between NDVI and LST (R^2 = 0.63, $p < 0.001$). The linear regression model indicates that for every 0.1 increase in NDVI, average LST decreases by approximately 2.1°C. Areas with NDVI below 0.1 experience average LST of 37.5°C, while areas with NDVI above 0.4 show average LST of 29.8°C—a difference of 7.7°C attributable to vegetation cover.

This correlation is particularly pronounced during midday hours when solar radiation is maximum. The cooling effect of vegetation is achieved through three mechanisms: (1) evapotranspiration, which converts sensible heat to latent heat; (2) shading, which reduces direct solar radiation absorption by surfaces; and (3) reduced thermal mass, as vegetated areas typically have lower heat capacity than built-up surfaces.

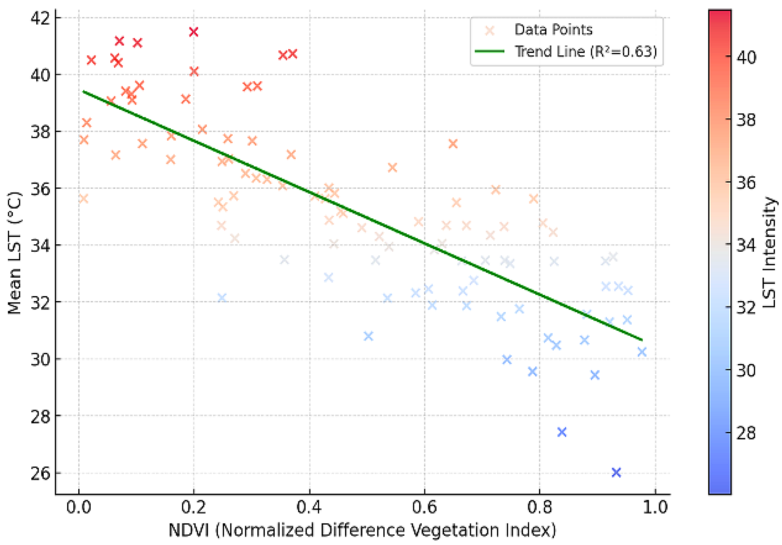

Figure 3: Scatter plot illustrating the inverse relationship between NDVI and mean LST in Southern Mehrabad Neighbourhood. The regression analysis (R^2 = 0.63) indicates a strong negative correlation, highlighting the cooling effect of vegetation cover on surface (Source: authors).

5.4 LST Variation by Land Use Type

Zonal statistics reveal temperature differences across land use categories, summarized in Table 1.

Table 1. Mean LST by land use category in Southern Mehrabad (summer averages, 2014–2024) (Source: authors).

Land use category	Mean LST (°C)
Commercial areas	37.2
Industrial zones	36.8
Vacant lots	36.5
Mixed residential	30.2
Educational/religious facilities	28.9
Parks and recreational areas	27.4

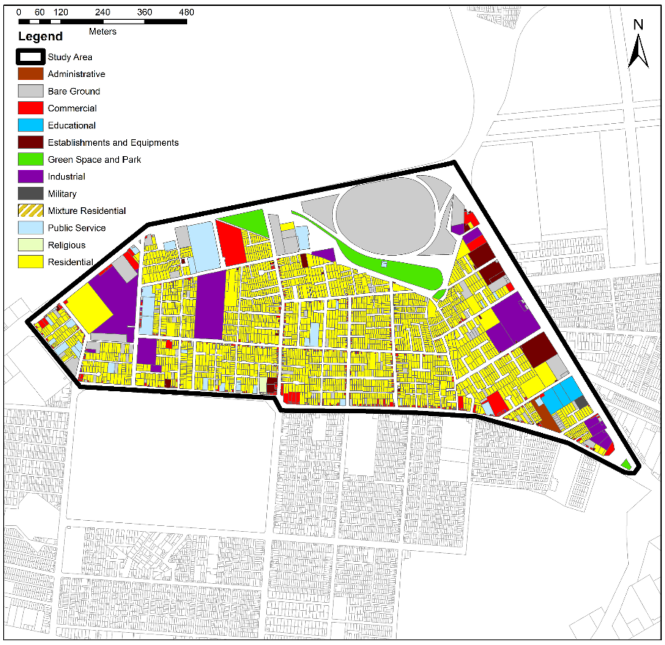

Figure 4. The land use type of the Southern Mehrabad Neighbourhood (source: authors).

Commercial and industrial areas record the highest mean LST values, while parks and recreational areas exhibit the lowest temperatures.

Figure 4 illustrates the spatial distribution of land use types across the Southern Mehrabad neighbourhood, showing a concentration of commercial and industrial functions along the southern and eastern edges, where higher temperatures are observed. In contrast, vegetated and mixed residential areas are more centrally distributed and correspond to relatively lower LST values. This relationship is further supported by Figure 5, which presents the distribution of mean LST across different land use categories, highlighting clear variability and clustering of higher temperature values within commercial, industrial, and vacant land types. Notably, commercial and industrial land uses exhibit LST values approximately 8–10°C higher than parks and green spaces. This disparity reflects differences in surface materials (e.g., asphalt and concrete versus vegetation), building density, and anthropogenic heat generation associated with commercial activities and industrial processes. Together, these results demonstrate that land use plays a critical role in shaping the spatial patterns of urban heat, with built-up and low-vegetation areas contributing most significantly to elevated surface temperatures.

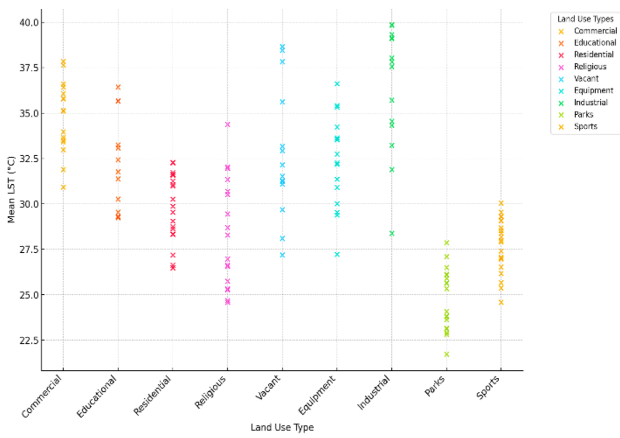

Figure 5. Distribution of mean LST across different land use types in Southern Mehrabad Neighbourhood (Source: authors).

5.5 Identification of Thermal Hotspots Through Hot Spot Analysis

Thermal hotspots were identified through spatial analysis of LST maps, focusing on areas that consistently exhibited the highest temperature values across the study period. Six major hotspot zones were delineated based on their persistent thermal intensity and spatial concentration, as summarized in Table 2. These hotspots collectively represent approximately 35% of the total neighbourhood area but account for the majority of extreme heat exposure affecting residents. Their recurrence across multiple years indicates structural thermal vulnerability rather than temporary fluctuations, making them priority targets for climate-responsive cooling interventions.

Table 2. Statistically significant thermal hotspots identified through spatial analysis of LST maps (Source: authors).

#	Location	Extent	Mean LST (°C)
1	Commercial strip along southern boundary (Shahid Eghbali Street)	450 m long	38.5
2	Eastern industrial zone near airport perimeter	0.3 km^2	37.8
3	Northern vacant lots	0.25 km^2	37.2
4	Shamshiri Street corridor (south)	380 m	36.9
5	Abdollahi Street (west) — isolated industrial buildings	—	36.5
6	Southeast vacant area	0.18 km^2	36.3

6 Discussion

6.1 Comparison with International Remote Sensing Studies

The strong inverse correlation between NDVI and LST (R^2 = 0.63) observed in Southern Mehrabad aligns with findings from comparable studies in Global South cities. Research in Patna, India documented even stronger correlations (R^2 > 0.90) (Yadav et al., 2023), while studies in Khanaqin, Iraq reported moderate relationships (R^2 = 0.28) during peak summer (Nasraldin et al., 2024).

Similar patterns have also been observed in other arid and semi-arid urban contexts in the Middle East and North Africa, where limited vegetation cover and high solar radiation intensify surface temperatures. Studies in cities such as Riyadh, Dubai, and Cairo have similarly identified strong spatial associations between low vegetation density and elevated land surface temperatures, reinforcing the role of green infrastructure as a critical cooling mechanism in hot-climate cities. The variation in correlation strength reflects differences in local climate conditions, vegetation types, and water availability for evapotranspiration.

Tehran's semi-arid climate and limited water resources constrain vegetation growth, yet the measured cooling effect of 2.1°C per 0.1 NDVI increase demonstrates significant potential for green infrastructure interventions. This cooling magnitude is comparable to findings in Banyuwangi, Indonesia, where dense vegetation reduced LST through evapotranspiration and shading mechanisms (Yu et al., 2018).

6.2 Land Use Patterns and Thermal Performance

The identification of commercial and industrial zones as primary thermal hotspots (LST > 37°C) is consistent with research in Jiaozuo, China, which found industrial areas to be major heat contributors (Jia et al., 2021), and Seoul, South Korea, where commercial uses showed elevated temperatures compared to residential and mixed-use areas. These patterns reflect the thermal properties of materials used in commercial and industrial construction—predominantly concrete, asphalt, and metal—which have high thermal mass and low albedo.

The superior thermal performance of mixed-use residential areas (mean LST 30.2°C) compared to single-use commercial zones (37.2°C) suggests that functional diversity and integration of green spaces can moderate surface temperatures. This finding has implications for land use planning in vulnerable neighbourhoods, indicating that conversion of monofunctional industrial zones to mixed-use developments with integrated vegetation could reduce thermal stress.

6.3 Implications for Data-Poor Contexts and Resource-Constrained Settings

This study demonstrates that satellite remote sensing can provide robust thermal diagnostics in contexts where ground-based monitoring infrastructure is limited. The validation exercise showed strong agreement (R^2 = 0.78) between satellite-derived LST and field measurements, confirming the reliability of Landsat data for neighbourhood-scale analysis in Tehran's climate.

The freely available nature of Landsat imagery and the accessibility of Google Earth Engine for cloud-based processing make this methodology replicable in other under-resourced urban contexts across the Global South. The approach requires minimal investment in ground equipment while providing comprehensive spatial coverage—a critical advantage in cities where climate adaptation budgets are constrained.

Furthermore, the identification of persistent thermal hotspots through multi-year analysis enables evidence-based prioritization of interventions. Rather than distributing limited resources evenly, planners can target specific geographic areas (e.g., the southern commercial strip, northern vacant lots) where thermal vulnerability is most acute and where interventions would have maximum impact on resident exposure.

6.4 Study Limitations and Future Research Directions

Several limitations should be acknowledged. First, this study focused exclusively on summer imagery to capture peak UHI conditions, but seasonal analysis across all months would provide a more comprehensive understanding of annual thermal dynamics. Second, Landsat's 100-meter thermal resolution (resampled to 30 meters for visualization), while appropriate for neighbourhood-scale analysis, introduces limitations when applied to fine-grained urban interventions. The spatial resolution may not capture micro-scale thermal variations at the street or building level, which are critical for detailed urban design strategies. As a result, while the analysis effectively identifies broader hotspot zones, caution should be exercised when translating these findings into site-specific interventions.

Third, satellite-derived LST represents surface temperature, not air temperature experienced by residents. While surface UHI is strongly correlated with atmospheric UHI, the relationship is not linear and varies by time of day and surface characteristics. Future research should integrate LST data with air temperature measurements and thermal comfort indices such as Physiological Equivalent Temperature (PET) or Universal Thermal Climate Index (UTCI) to directly assess human heat exposure.

Finally, higher-resolution satellite platforms (e.g., ECOSTRESS with 70-meter thermal resolution, or commercial high-resolution imagery) could provide finer-scale thermal mapping, though at higher cost. Machine learning approaches could also be explored to model LST from multispectral imagery, potentially enabling more frequent temporal monitoring. Future research could benefit from higher-resolution thermal data or UAV-based measurements to improve the precision of micro-scale urban heat assessments.

7 Conclusion

This study presented a comprehensive remote sensing-based assessment of Urban Heat Island vulnerability in Southern Mehrabad, Tehran—a socioeconomically disadvantaged neighbourhood facing compound environmental stresses from proximity to Mehrabad Airport and rapid urbanization. Using ten years of Landsat 8/9 satellite imagery, we systematically mapped Land Surface Temperature and vegetation cover patterns, identified persistent thermal hotspots, and quantified the cooling effect of green infrastructure.

Key findings include: (1) a strong inverse relationship between NDVI and LST ($R^2 = 0.63$), demonstrating that vegetation provides measurable cooling of approximately 2.1°C per 0.1 NDVI increase; (2) identification of commercial and industrial zones as primary thermal hotspots, with temperatures 8–10°C higher than vegetated areas; (3) documentation of severe vegetation deficiency, with 65% of the neighbourhood exhibiting minimal green cover; and (4) validation of satellite-derived thermal maps through field measurements, confirming their reliability for neighbourhood-scale climate diagnostics.

The methodology demonstrated here—combining freely available Landsat imagery, cloud-based processing on Google Earth Engine, and spatial analysis in ArcGIS—offers a replicable framework for UHI assessment in data-poor contexts across the Global South. By providing spatial evidence of thermal vulnerability at fine geographic scales, this approach enables targeted, evidence-based allocation of limited climate adaptation resources to neighbourhoods and population groups most exposed to extreme heat.

For Southern Mehrabad specifically, results indicate that priority interventions should target: (1) the southern commercial strip along Shahid Eghbali Street, where high pedestrian exposure coincides with extreme surface temperatures; (2) northern and southeastern vacant lots, which could be transformed into green infrastructure; and (3) eastern industrial zones, where conversion to mixed-use development with integrated vegetation would reduce both thermal stress and land use incompatibility.

Future research should expand this thermal diagnostic framework to include: (1) higher temporal resolution monitoring to capture diurnal and seasonal LST variations; (2) integration with demographic and health data to assess population-weighted heat exposure; (3) scenario modelling to evaluate the cooling potential of specific intervention strategies; and (4) comparative analysis across multiple vulnerable neighbourhoods in Tehran and other Middle Eastern cities to identify generalizable patterns and context-specific adaptation needs. Additionally, integrating demographic and health-related datasets would allow for a more comprehensive assessment of heat vulnerability and environmental justice impacts.

Ultimately, this study contributes to the growing body of evidence demonstrating that satellite remote sensing, when combined with spatial analysis and field validation, can systematically identify urban heat vulnerabilities and inform climate-responsive planning in under-resourced neighbourhoods. As global temperatures continue to rise and cities in the Global South face escalating heat risks, such data-driven diagnostic tools become increasingly essential for protecting vulnerable populations and promoting environmental justice.

Ethical Approval Declaration

Not Applicable

Informed Consent Statement

Not Applicable

Acknowledgements

The authors gratefully acknowledge Tehran Municipality and the Iran Meteorological Organization for providing ancillary spatial and environmental data, and the Google Earth Engine team for open access to cloud-based Landsat processing.

Funding

This research received no specific grant from any funding agency in the public, commercial, or not-for-profit sectors.

Data Availability Statement

Landsat 8/9 imagery used in this study is openly available through the USGS EarthExplorer portal and Google Earth Engine catalog. Derived LST and NDVI products, together with field-validation records, are available from the corresponding author upon reasonable request.

Conflicts of Interest

The authors declare no conflict of interest.

References

Amirtham, L., & Devadas, M. (2007). Impact of built environment on outdoor thermal conditions in the hot humid city of Chennai. In *Proceedings of International Conference on Sustainable Building Southeast Asia*. Malaysia.

Azizdoost, A., Shababani, M., & Seraji Aghdam, S. (2019). The livability measurements in the old urban fabric of zone 1 in district 9, Tehran. *Socio-Spatial Studies*, *3*(5), 50–65.

Bowler, D. E., Buyung-Ali, L., Knight, T. M., & Pullin, A. S. (2010). Urban greening to cool towns and cities: A systematic review of the empirical evidence. *Landscape and Urban Planning*, *97*(3), 147–155. https://doi.org/10.1016/j.landurbplan.2010.05.006

EPA. (2023). Urban heat island effect. U.S. EPA. Retrieved 7 June 2023, from https://www.epa.gov/heatislands/urban-heat-island-effect

EPA. (2025a). Heat island trends. U.S. EPA. Retrieved 20 July 2025, from https://www.epa.gov/heatislands/heat-island-trends.

Gartland, L. (2012). *Heat islands: Understanding and mitigating heat in urban areas*. Routledge.

ILO. (2019). *Increase in heat stress predicted to bring productivity loss equivalent to 80 million jobs*. International Labour Organization. Retrieved from https://www.ilo.org/resource/news/increase-heat-stress-predicted-bring-productivity-loss-equivalent-80

IPCC. (2022). *Climate change 2022: Impacts, adaptation and vulnerability. Contribution of Working Group II to the Sixth Assessment Report of the Intergovernmental Panel on Climate Change*. Cambridge University Press. Retrieved from https://www.ipcc.ch/report/ar6/wg2/

IPCC. (2023). *Climate change 2023: Synthesis report. Contribution of Working Groups I, II and III to the Sixth Assessment Report of the Intergovernmental Panel on Climate Change*. Retrieved from https://www.ipcc.ch/report/ar6/syr/

Jia, W., Zhao, S., Zhang, X., Liu, S., Henebry, G. M., & Liu, L. (2021). Urbanization imprint on land surface phenology: The urban-rural gradient analysis for Chinese cities. *Global Change Biology*, *27*(12), 2895–2904. https://doi.org/10.1111/gcb.15602

Jones, P., Groisman, P. Y., Coughlan, M., Plummer, N., Wang, W. C., & Karl, T. R. (1990). Assessment of urbanization effects in time series of surface air temperature over land. *Nature*, *347*(6289), 169–172. https://doi.org/10.1038/347169a0

Kjellström, T., Briggs, D., Freyberg, C., Lemke, B., Otto, M., & Hyatt, O. (2016). Heat, human performance, and occupational health: A key issue for the assessment of global climate change impacts. *Annual Review of Public Health*, *37*, 97–112. https://doi.org/10.1146/annurev-publhealth-032315-021740

Kong, F., Yin, H., James, P., Hutyra, L. R., & He, H. S. (2014). Effects of spatial pattern of greenspace on urban cooling in a large metropolitan area of eastern China. *Landscape and Urban Planning*, *128*, 35–47. https://doi.org/10.1016/j.landurbplan.2014.04.018

NASA. (2025). 2024 was the warmest year on record. NASA Earth Observatory. Retrieved from https://earthobservatory.nasa.gov/images/153806/2024-was-the-warmest-year-on-record

Nasraldin, H., Nasir, S., & Nasraldin, H. (2024). Remote sensing-based analysis of LST and NDVI correlation for the coolest and hottest month of 2023 in Khanaqen City. *Journal of University of Raparin*, *11*, 898–914.

NLC, National League of Cities. (2023). Urban heat island effect solutions and funding. Retrieved from https://www.nlc.org/article/2023/02/13/urban-heat-island-effect-solutions-and-funding/

Oke, T. R. (1982). The energetic basis of the urban heat island. *Quarterly Journal of the Royal Meteorological Society*, *108*(455), 1–24. https://doi.org/10.1002/qj.49710845502

Oke, T. R., Mills, G., Christen, A., & Voogt, J. A. (2017). *Urban climates*. Cambridge University Press

Rizwan, A. M., Dennis, L. Y., & Chunho, L. (2008). A review on the generation, determination and mitigation of urban heat island. *Journal of Environmental Sciences*, *20*(1), 120–128. https://doi.org/10.1016/S1001-0742(08)60019-4

Roshan, G., Sarli, R., & Grab, S. W. (2021). The case of Tehran's urban heat island, Iran: Impacts of urban 'lockdown' associated with the COVID-19 pandemic. *Sustainable Cities and Society*, *75*, 103263. https://doi.org/10.1016/j.scs.2021.103263

Smith, K. R., Woodward, A., Campbell-Lendrum, D., Chadee, D., Honda, Y., Liu, Q., ... Aranda, C. (2014). Climate change 2014: Impacts, adaptation, and vulnerability. Part A: Global and sectoral aspects. In *Contribution of Working Group II to the Fifth Assessment Report of the Intergovernmental Panel on Climate Change*. Cambridge University Press. https://www.ipcc.ch/report/ar5/wg2/

Sodoudi, S., Shahmohamadi, P., Vollack, K., Cubasch, U., & Che-Ani, A. (2014). Mitigating the urban heat island effect in megacity Tehran. *Advances in Meteorology*, *2014*(1), 547974. https://doi.org/10.1155/2014/547974

Stewart, I. D., & Oke, T. R. (2012). Local climate zones for urban temperature studies. *Bulletin of the American Meteorological Society*, *93*(12), 1879–1900. https://doi.org/10.1175/BAMS-D-11-00019.1

Stone Jr, B., Mallen, E., Rajput, M., Gronlund, C. J., Broadbent, A. M., Krayenhoff, E. S., ... Georgescu, M. (2021). Compound climate and infrastructure events: How electrical grid failure alters heat wave risk. *Environmental Science & Technology*, *55*(10), 6957–6964. https://doi.org/10.1021/acs.est.1c00024

UN, United Nations Environment Programme. (2021). *Beating the heat: A sustainable cooling handbook for cities*. UNEP.

Weng, Q. (2003). Fractal analysis of satellite-detected urban heat island effect. *Photogrammetric Engineering & Remote Sensing*, *69*(5), 555–566. https://doi.org/10.14358/PERS.69.5.555

WHO. (2014). *Quantitative risk assessment of the effects of climate change on selected causes of death, 2030s and 2050s*. World Health Organization. https://www.who.int/publications/i/item/9789241507691

WHO. (n.d.). Heatwaves. World Health Organization. Retrieved 9 June from https://www.who.int/health-topics/heatwaves#tab=tab_1

WMO, World Meteorological Organization. (2025). WMO confirms 2024 as warmest year on record at about 1.55 °C above pre-industrial level. Retrieved from https://wmo.int/news/media-centre/wmo-confirms-2024-warmest-year-record-about-155degc-above-pre-industrial-level

Yadav, A., Kumar, R., & Swarup, S. (2023). Remote sensing image-based analysis of the urban heat island effect in relation to the normalized difference vegetation index (NDVI): A case study of Patna Municipal Corporation. *International Journal of Research in Applied Science and Engineering Technology*, *11*(1), 1143–1155. https://doi.org/10.22214/ijraset.2023.48793

Yu, Z., Guo, X., Zeng, Y., Koga, M., & Vejre, H. (2018). Variations in land surface temperature and cooling efficiency of green space in rapid urbanization: The case of Fuzhou city, China. *Urban Forestry & Urban Greening*, *29*, 113–121. https://doi.org/10.1016/j.ufug.2017.11.008

Zhang, H., Arens, E., & Pasut, W. (2011). Air temperature thresholds for indoor comfort and perceived air quality. *Building Research & Information*, *39*(2), 134–144. https://doi.org/10.1080/09613218.2011.552703